0022-3565/11/3391-62–71$25.00
THE JOURNAL OF PHARMACOLOGY AND EXPERIMENTAL THERAPEUTICS
JPET 339:62–71, 2011

Vol. 339, No. 1
184671/3715217
Printed in U.S.A.

Generation and Characterization of a *Cyp2f2*-Null Mouse and Studies on the Role of CYP2F2 in Naphthalene-Induced Toxicity in the Lung and Nasal Olfactory Mucosa[S]

Lei Li, Yuan Wei, Laura Van Winkle, Qing-Yu Zhang, Xin Zhou, Jinping Hu, Fang Xie, Kerri Kluetzman, and Xinxin Ding

Wadsworth Center, New York State Department of Health, and School of Public Health, State University of New York at Albany, Albany, New York (L.L., Y.W., Q.-Y.Z., X.Z., J.H., F.X., K.K., X.D.); and Center for Health and the Environment, University of California Davis, Davis, California (L.V.W.)

Received May 31, 2011; accepted June 23, 2011

ABSTRACT

The CYP2F enzymes, abundantly expressed in the respiratory tract, are active toward many xenobiotic compounds, including naphthalene (NA). However, the precise roles of these enzymes in tissue-selective chemical toxicity have been difficult to resolve. A *Cyp2f2*-null mouse was generated in this study by disrupting the *Cyp2f2* fourth exon. Homozygous *Cyp2f2*-null mice, which had no CYP2F2 expression and showed no changes in the expression of other P450 genes examined, were viable and fertile and had no in utero lethality or developmental deficits. The loss of CYP2F2 expression led to substantial decreases in the in vitro catalytic efficiency of microsomal NA epoxygenases in lung (up to ~160-fold), liver (~3-fold), and nasal olfactory mucosa (OM; up to ~16-fold), and significant decreases in rates of systemic NA (300 mg/kg i.p.) clearance. The *Cyp2f2*-null mice were largely resistant to NA-induced cytotoxicity, when examined at 24 h after NA dosing (at 300 mg/kg i.p.), and to NA-induced depletion of total nonprotein sulfhydryl (NPSH), examined at 2 h after dosing, in the lungs. In contrast, the loss of CYP2F2 expression did not alleviate NA-induced NPSH depletion or tissue toxicity in the OM. Mouse CYP2F2 clearly plays an essential role in the bioactivation and toxicity of NA in the lung but not in the OM. The *Cyp2f2*-null mouse should be valuable for studies on the role of CYP2F2 in the metabolism and toxicity of numerous other xenobiotic compounds and for future production of a *CYP2F1*-humanized mouse.

Introduction

Cytochrome P450 (P450)-catalyzed metabolic activation is highly relevant to respiratory tract injury caused by numerous environmental chemicals, drugs, and other xenobiotic compounds, which enter the body through either the airway or other portals and are present in the systemic circulation. Various P450 enzymes, including members of the *CYP2F* subfamily, which are preferentially expressed in the respiratory tract, are active toward pulmonary toxicants or procarcinogens (Buckpitt et al., 2002; Hukkanen et al., 2002). Recombinant CYP2F enzymes, including human CYP2F1, mouse CYP2F2, goat CYP2F3, and rat CYP2F4, have been studied in heterologous expression systems, and one or more of these enzymes have been found to be capable of bioactivating various pulmonary toxicants, including naphthalene (NA), 2-methylnaphthalene, 1-nitronaphthalene, styrene, 3-methylindole, benzene, trichloroethylene, dichloroethylene, and benzo(*a*)pyrene (for a recent review, see Zhang and Ding, 2008). However, the relative contribution of CYP2F enzymes to the bioactivation of respiratory tract toxicants remained elusive and merely correlative, due largely to the lack of specific chemical inhibitors or knockout animal models.

NA is the most abundant polycyclic aromatic hydrocarbon in ambient urban air (Arey et al., 1987) and is released by

This work was supported in part by the National Institutes of Health National Institute of Environmental Health Sciences [Grants ES004311, ES012720, ES007462]; the National Institutes of Health National Cancer Institute [Grant CA092596], the National Institutes of Health National Institute of General Medical Sciences [Grant GM082978]; and a grant from the Styrene Information and Research Center.

L.L. and Y.W. contributed equally to this work.

Article, publication date, and citation information can be found at http://jpet.aspetjournals.org.
doi:10.1124/jpet.111.184671.

[S] The online version of this article (available at http://jpet.aspetjournals.org) contains supplemental material.

ABBREVIATIONS: P450, cytochrome P450; NA, naphthalene; ES, embryonic stem; B6, C57BL/6; WT, wild type; NPSH, nonprotein sulfhydryl; OM, nasal olfactory mucosa; AP, acetaminophen; kbp, kilobase pair(s); PCR, polymerase chain reaction; bp, base pair(s); MS, mass spectrometry; CCSP, Clara cell secretory protein; AUC, area under the concentration-time curve; GC-MS, gas chromatography-mass spectrometry; LCN, liver-*Cpr*-null; C_{max}, maximal concentration; neo, neomycin-resistance gene.

combustion of wood, gasoline, diesel, and tobacco. The pulmonary toxicity of NA has been studied extensively. NA-induced toxicity shows high tissue and species selectivity. It primarily targets Clara cells (nonciliated bronchiolar epithelial cells) lining the airway epithelium of the mouse, causing cytotoxicity after short-term exposure via either inhalation or parenteral routes (Plopper et al., 1992; West et al., 2001). NA treatment also leads to acute cytotoxicity in the nasal mucosa (Plopper et al., 1992). According to the International Agency for Research on Cancer, NA is a *possible human carcinogen*, a designation supported by the results of the National Toxicology Program chronic rodent bioassays for NA, which found significant, dose-dependent increases in alveolar adenomas in the lungs of female mice, and in adenomas and neuroblastomas of the nasal epithelium in rats (Abdo et al., 1992, 2001). The mechanism of NA carcinogenicity is thought to involve repeated cycles of injury and repair related to acute cytotoxicity after bioactivation of NA by P450 enzymes (Brusick 2008).

In the lung, the sensitivity of the Clara cells to NA is presumed to be related to efficient metabolic activation catalyzed by CYP2F enzymes localized within these cells (Buckpitt et al., 1995). Mouse CYP2F2 has high catalytic efficiency toward NA (K_m, $\sim$ 3 μM; V_{max}, 104 nmol · min^{-1} · nmol $P450^{-1}$) in vitro (Shultz et al., 1999). Early in vivo studies in rodents demonstrated a correlation between the covalent binding of reactive NA metabolites and glutathione depletion (Buckpitt and Warren, 1983). P450 inhibition decreased covalent binding and toxicity, whereas glutathione depletion increased it (Warren et al., 1982; Phimister et al., 2004). However, direct evidence for the role of CYP2F2 in mediating the respiratory tract toxicity of NA has yet to be obtained, and the question is still unresolved whether CYP2F2 is the key enzyme in NA metabolic activation in vivo. The latter question is pertinent, given the fact that several other P450 enzymes expressed in the respiratory tract, including CYP1A, -2A, -2B, -2E, and -3A, are also active in NA bioactivation (Buckpitt et al., 2002; Fukami et al., 2008; Lin et al., 2009).

In this study, a novel *Cyp2f2*-null mouse was generated through homologous recombination in embryonic stem (ES) cells derived from the C57BL/6 (B6) mouse strain. Homozygous *Cyp2f2*-null mice were characterized for viability and fertility, growth rates, Clara cells distribution and development, and potential compensatory expression of other enzymes that may be involved in NA bioactivation. The *Cyp2f2*-null mice were compared with wild-type (WT) mice for efficiency of microsomal NA metabolic activation in vitro, as well as rates of systemic NA clearance and extent of NA-induced tissue toxicity in vivo, at NA doses established previously to induce respiratory toxicity in WT mice. The extent of NA-induced lung and OM toxicity was assessed by histological analysis and through measurements of tissue levels of nonprotein sulfhydryl (NPSH). The results of our studies not only establish the *Cyp2f2*-null mouse as a valuable model for studies on the role of CYP2F2 in the metabolism and toxicity of numerous xenobiotic compounds but also provide novel and definitive evidence that CYP2F2 plays an essential role in the bioactivation and toxicity of NA in the lung, but not in the nasal olfactory mucosa (OM).

Materials and Methods

Chemicals and Reagents. NA (99% pure), NA-d_8 (99% pure), corn oil (highly refined, low acidity), GSH, and NADPH were purchased from Sigma Aldrich (St. Louis, MO). Acetaminophen-glutathione (AP-GSH) was purchased from Toronto Research Chemicals (Toronto, ON, Canada). NA-GSH standard, consisting of a mixture of all four stereoisomers, and prepared as described previously (Buckpitt et al., 1987), was a generous gift from Drs. Alan R. Buckpitt and Dexter Morin (University of California at Davis, Davis, CA). Unless otherwise stated, all solvents (dichloromethane, formic acid, methanol, and water) were of analytical grade (Fisher Scientific, Houston, TX).

Generation of the *Cyp2f2*-Null Mouse. A bacterial artificial chromosome clone containing the *Cyp2f2* gene from the B6 mouse strain (ID number RP23-148D9) was obtained from BACPAC Resources (Oakland, CA). A 1.7-kbp SmaI-BstEII fragment (containing *Cyp2f2* exons 2 and 3) and a 8.0-kbp ApaI-SalI fragment (containing *Cyp2f2* exons 5–9 and a loxP site) were inserted into the pGK-neo-tk vector (Zhuo et al., 2004) for preparation of the targeting construct. The targeting vector was linearized with SalI before electroporation into ES cells.

The Bruce4 (B6-derived) ES cells (Köntgen et al., 1993), kindly provided by Dr. Colin Stewart (National Cancer Institute, Frederick, MD), were used for electroporation, at the University of Michigan Transgenic Animal Model Core (Ann Arbor, MI). Positive ES cell clones were identified by PCR, using the primers F1 (5′-gaaccagtgttttggtagatgg-3′; upstream of the 1.7-kbp SmaI-BstEII fragment) and R1 (5′-cagacttttggttttggatgg-3′; within the vector region) and was confirmed by Southern blot analysis with both internal (a 1.0-kbp fragment, beginning at ~700 bp upstream of the neo start codon) and external (a 0.9-kbp fragment located ~300 bp upstream of *Cyp2f2* exon 2) probes.

ES cells from positive clones were injected into the blastocysts from albino B6(Cg)-Tyr^{c-2J}/J (The Jackson Laboratory, Bar Harbor, ME) female mice at the Transgenic and Knockout Core Facility of the Wadsworth Center. Blastocysts were transferred into the uterus of a pseudopregnant B6CBAF1/J mouse, for generation of offspring. Adult male chimeras were bred with B6 female mice to produce germline-transmission F1 mice that were heterozygous for the *Cyp2f2*-null allele. F2 homozygotes were used for breeding and characterization. Genotypic analysis of mouse tail DNA for targeted *Cyp2f2* allele was performed using the same primers as described above for PCR screening of ES cells. Primers for genotyping WT allele were F2 (5′-agagatgactcggtggctgt-3′) and R2 (5′-tttttcccatgccaaagttc-3′). Unless otherwise indicated, B6 mice were used as WT controls in all experiments described. All procedures involving animals were approved by the Institutional Animal Care and Use Committee of the Wadsworth Center.

RNA-PCR Analysis of CYP2F2 Expression. Total RNA was isolated with use of the RNeasy Mini kit (QIAGEN, Valencia, CA) and was treated with DNase I (Invitrogen, Carlsbad, CA) before reverse transcription. RNA-PCR analysis was performed as described previously (Zhou et al., 2010), with use of gene-specific PCR primers (5′-gttcagtggccgaggcga-3′ and 5′-ggtgagcagacgctcatcgtca-3′; annealing temperature of 60°C) for amplification of a 310-bp fragment corresponding to *Cyp2f2* exons 3 through 5. PCR products were analyzed on 1% agarose gels and visualized by staining with ethidium bromide. A 100-bp DNA marker (Invitrogen) was used for size determination.

Immunoblot Analysis of P450 Expression. Immunoblot analysis was carried out essentially as described previously (Ding and Coon, 1990); the intensity of the detected bands was quantified through the use of an imaging densitometer (GS-710; Bio-Rad Laboratories, Hercules, CA). The expression of CYP2A, CYP1A, CYP2B, CYP2E, and CYP3A proteins was analyzed using the following antibodies: rabbit anti-mouse CYP2A5 (Gu et al., 1998), goat anti-rat CYP1A1/2, goat anti-rat 2B1/2, (BD Gentest, Woburn, MA), rabbit

anti-rat CYP2E1 (AKELA Pharma Inc., Montreal, QC, Canada), and rabbit anti-rat CYP3A (Enzo Life Sciences, Inc., Plymouth Meeting, PA). Expression of CYP2F2 protein was analyzed with a rabbit anti-CYP2F anti-peptide antibody (custom-prepared by GenScript, Piscataway, NJ); heterologously expressed human CYP2F1 protein contained in an Sf9 cell microsomal preparation was used as a positive control for immunoblot analysis. Calnexin, a marker protein for the endoplasmic reticulum, was detected using a rabbit anti-human calnexin antibody (GenScript).

Determination of Plasma Levels of NA and NA-GSH. Mice were given a single injection of NA (at 300 mg/kg i.p.) in corn oil. Blood samples were collected from the tail at various times (15 min–8 h) after the injection for preparation of plasma. Tissues from individual mice were homogenized at room temperature in microsome preparation buffer (0.1 M Tris-acetate buffer, containing 0.15 M KCl and 1.0 mM EDTA, pH 7.4) (Ding and Coon, 1990), at a w/v ratio of 1 g liver or lung per 3 ml of buffer or one pool of dissected OM (~20 mg, from one mouse) in 0.6 ml of buffer, using a Polytron (model GT 10–35; Kinematica, Bohemia, NY).

For determination of NA-GSH, each plasma sample (10 μl) or tissue homogenate sample (50 μl) was spiked with 2 ng of AP-GSH (in 10 μl of methanol) as an internal standard and then mixed with 90 μl of methanol to precipitate protein. Aliquots (5 μl each) of the supernatant were used for analysis. NA-GSH was determined with a liquid chromatography-MS/MS system consisted of an Agilent 1200 Series high performance liquid chromatography, fitted with an Atlantis T3 column (2.1 × 100 mm, 3 μm; Waters, Milford, MA) and an ABI 4000 Q-Trap mass spectrometer (Applied Biosystems, Foster City, CA). The mobile phase consisted of solvent A (0.1% formic acid in water) and solvent B (0.1% formic acid in methanol). The analytes were eluted, at a flow rate of 0.2 ml/min, using a linear gradient from 10% B to 80% B (between 0 and 8 min), followed by a hold at 80% B for 2 min. The chromatographic condition did not permit baseline separation of various NA-GSH stereoisomers in the authentic standard; therefore, all stereoisomers were quantitated as a single analyte. The mass spectrometer was set for multiple-reaction monitoring and was operated in a positive-ion mode with an electrospray ionization source. Nitrogen was used as the curtain gas and the collision gas. The ion-spray voltage was set at 5000 V, the gas temperature at 400°C, and the declustering and entrance potentials at 50 and 10 V, respectively. The transition ion pair of *m/z* 452/306 (loss of a hydroxyl and a pyroglutamate group) was used for NA-GSH quantitation, whereas 452/434 (for the dehydration product) was used for NA-GSH confirmation (Buckpitt et al., 1987). The collision energy and collision cell exit potential for the *m/z* 452/306 transition were set to 25 and 10 V, respectively. The transition ion pair for quantitation of the internal standard (AP-GSH) was 457/328 (Bartha et al., 2010) with the collision energy and collision cell exit potential set as 30 and 10 V, respectively. The retention time for NA-GSH was ~10.18 min and that for AP-GSH was ~8.90 min. NA-GSH standard (0.05–20 μg/ml), as well as the internal standard, were added to blank mouse plasma to construct calibration curve. The recoveries of added standards in blank plasma or tissue homogenates were >80% at all concentrations tested.

For determination of NA, each plasma sample (10 μl) or tissue homogenate sample (50 μl) was spiked with 5 ng of NA-d_8 (in 10 μl of methanol) as an internal standard. The resultant mixture was extracted with 100 μl of dichloromethane. All procedures were carried out in sealed tubes to prevent NA evaporation. Aliquots of the dichloromethane extract (1 μl each) was analyzed on an Agilent GC-MS system, consisting of a model 7890A GC, a model 5975C MS, and an HP-5 (30-m × 0.25-mm × 0.25-μm) column. The GC-MS conditions were modified from a method described previously (Cho et al., 2006). The temperature gradient consisted of an initial hold at 40°C for 1 min, linear increases to 100°C at 25°C/min, then to 150°C at 10°C/min, and to 300°C at 30°C/min. Samples were injected in splitless mode, with injector temperature at 260°C and carrier gas (helium) flow at 1 ml/min. The MS conditions were as follows: ion source temperature, 230°C; ionization energy, 70 eV; emission current, 60 μA; and accelerating voltage, 1.5 kV. The GC-MS was operated in the positive electron ionization mode. Quantitation was carried out in selected ion monitoring mode, with peak area measurement, and with *m/z* 128 for NA and *m/z* 136 for NA-d_8. The retention time for NA-d_8 was ~7.09 min and that for NA was ~7.12 min. NA standard (0.05–20 μg/ml), as well as NA-d_8, were added to blank mouse plasma to construct calibration curve. The recoveries were >85% at all concentrations tested.

Assays for NA Metabolism in Vitro. Microsomal metabolic activation of NA was assayed by a determination of the rates of formation of NA-GSH, essentially as described previously (Shultz et al., 1999). Reaction mixtures contained 50 mM phosphate buffer, pH 7.4, 2.5~400 μM NA (added in 2 μl of methanol), 10 mM GSH, 0.2 mg/ml (for liver and lung), or 0.05 mg/ml (for OM) microsomal protein, and 1 mM NADPH, in a final volume of 0.2 ml. The reaction was carried out in sealed tubes at 37°C for 5 min and quenched by an addition of 2 volumes of ice-cold methanol (containing 0.5 ng of AP-GSH as internal standard). The resultant mixture was centrifuged to remove precipitated protein, and aliquots of the supernatant were used for NA-GSH determination, as described above. In control incubations, the reaction was quenched before the addition of NADPH.

Histopathological Examination. Tissues were fixed in 10% neutral buffered formalin (for liver and lung) or in Bouin's solution (for nose) and then sectioned and stained with hematoxylin and eosin for pathological examination, as described before (Gu et al., 2003, 2005). For in-depth histological analysis of the extent of lung toxicity, the lungs were pressure perfused with Karnovsky's fixative (Tousimis, Rockville, MD) at 30 cm for 1 h by intratracheal instillation, immersed in Karnovsky's fixative, embedded in epoxy resin (Araldite 502; Electron Microscopy Sciences, Hatfield PA), sectioned at 1 μm, and stained with methylene blue/Azure II (Plopper et al., 1992).

Immunohistochemical Analysis of Clara Cell Secretory Protein Expression. Immunohistochemical analysis of CCSP expression was conducted as described previously (Weng et al., 2007). The lungs were fixed in 10% formalin and embedded in paraffin. After deparaffinization and dehydration, tissue sections were subjected to antigen retrieval in citrate buffer at 95°C for 1 h (Dako Denmark A/S, Glostrup, Denmark). Sections were preincubated with normal goat serum (Invitrogen) for 60 min at room temperature to prevent nonspecific antibody binding and then with a rabbit anti-human CCSP antibody (1:2000 dilution; Biovendor, Candler, NC) at 4°C overnight. The Alexa Fluor 594-conjugated goat anti-rabbit secondary antibody (Invitrogen) was used to visualize the antigenic signal. For negative control sections, the primary antibody was omitted. Sections were mounted with Prolong Gold antifade reagent with 4,6-diamidino-2-phenylindole (Invitrogen). Stained sections were imaged using a Nikon Eclipse 50i fluorescence microscope (Nikon, Tokyo, JP).

Other Methods. All mice were obtained from breeding stocks maintained at the Wadsworth Center. The LCN [Alb-Cre(±)Cpr(lox/lox)] mice (Gu et al., 2003), which have tissue-specific deletion of the *Cpr* gene, and thus little P450 activity, in hepatocytes, and their WT littermates [Alb-Cre(−/−)Cpr(lox/lox)] were congenic on the B6 background. NPSH levels in liver, lung, and OM were determined as described previously (Tonge et al., 1998; Xie et al., 2010), with use of GSH as a standard. Lung, liver, and OM microsomes were prepared as described previously (Gu et al., 1997). Pharmacokinetic parameters were calculated using the WinNonlin software (Pharsight, Mountain View, CA). Enzyme kinetic parameters were calculated using Prism (GraphPad Software, San Diego, CA). Statistical significance of differences between two groups in various parameters was examined using Student's *t* test.

Results

Generation and Characterization of the *Cyp2f2*-Null Mouse. The structures of the WT *Cyp2f2* allele, the targeting construct, and the *Cyp2f2*-null allele are shown in Fig. 1A. The targeting vector contained, sequentially, a 1.7-kbp 5′-homology region corresponding to exons 2 and 3, the neomycin-resistance gene (neo) cassette in reverse direction, a loxP site, and an 8.0-kbp 3′-homology region containing exons 5 to 9. In the *Cyp2f2*-null allele, the *Cyp2f2* exon 4 (coding exon 3) was replaced by neo, through homologous recombination in ES cells derived from the B6 strain. Two positive clones (nos. 30 and 43) were selected for blastocyst injection; they did not contain random insertion of the targeting construct, as indicated by Southern blot analysis with both internal and external DNA probes (data not shown). Ten male chimeras were identified, three of which exhibited germline transmission after cross-breeding with WT B6 female mice. The germline-transmission F1 heterozygotes were then intercrossed to generate F2 homozygous *Cyp2f2*-null [*Cyp2f2*(−/−)] mice. Genotypes were confirmed by the presence of the characteristic bands for the WT (11.6-kbp) and the *Cyp2f2*-null (6.5-kbp) alleles on Southern blots (Fig. 1B). Absence of CYP2F2 mRNA and protein expression in the lungs of the null mice was confirmed by PCR and immunoblot analysis, respectively (Fig. 1C).

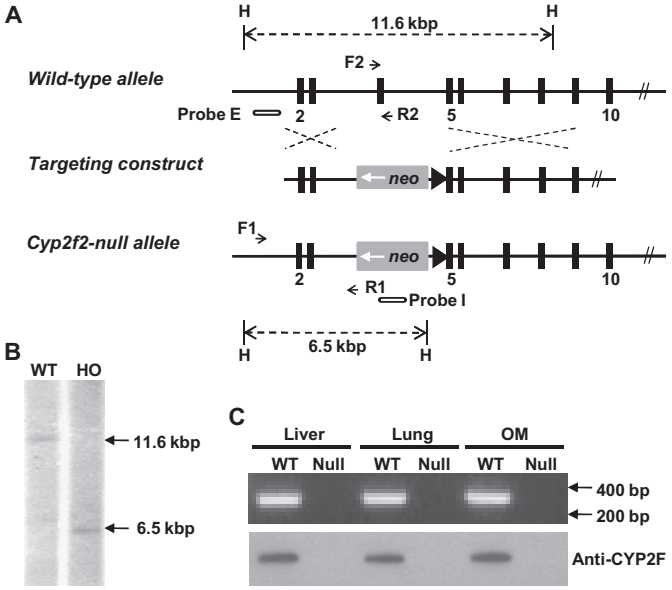

Fig. 1. Targeted disruption of the mouse *Cyp2f2* gene. A, structures of the WT *Cyp2f2* allele, the targeting vector, and the targeted *Cyp2f2* allele are shown. Triangles represent loxP sites; selected *Cyp2f2* exons (solid boxes) are numbered below. External (probe E, 0.9 kbp) and internal (probe I, 1.0 kbp) DNA probes used for Southern blot analysis are shown as open boxes. The diagnostic HindIII (H) fragments detected by the external probe in WT (11.6 kbp) and targeted (6.5 kbp) alleles, as well as positions of the PCR primers used for genotyping (F1 and R1 for *Cyp2f2* allele; F2 and R2 for WT allele), are indicated. B, Southern blot analysis of mouse genomic DNA. Thymus DNA (10 μg each) from WT and homozygous (HO) *Cyp2f2*-null mice were analyzed with use of probe E. The 11.6- and 6.5-kbp bands detected represent the WT *Cyp2f2* and the *Cyp2f2*-null alleles, respectively. C, absence of CYP2F2 mRNA and protein in the tissues of the *Cyp2f2*-null mice. RNA-PCR was performed using total RNA prepared from the liver, lung, and OM of adult male and female (two each, pooled) WT or *Cyp2f2*-null (Null) mice. PCR products were analyzed on an agarose gel and visualized by staining with ethidium bromide (top). The positions of selected fragments of a 100-bp DNA marker are indicated. Immunoblot analysis (bottom) was performed using a rabbit anti-CYP2F1/2 antibody on microsomal proteins from the liver, lung, and OM (5 μg/lane).

Homozygous *Cyp2f2*-null mice were fertile and normal in general appearance, and daily activities. Genotype frequency (number of pups with a given genotype/total number of pups born) among the pups derived from intercrosses between *Cyp2f2*(+/−) mice was 25% (28 of 112) for homozygotes [*Cyp2f2*(−/−)], 51% (57 of 112) for heterozygotes [*Cyp2f2*(+/−)], and 24% (27 of 112) for WT littermates [*Cyp2f2*(+/+)], with no significant difference among the three genotypes ($p > 0.05$, χ-squared test). The conformity of the genotype distribution with Mendelian distribution indicates absence of embryonic lethality among the null mice. Adult body and organ weights (liver, kidney, lung, brain, testis, and heart for male mice; liver, kidney, lung, brain, and heart for female mice) were similar in *Cyp2f2*-null and WT B6 mice (Supplemental Table 1), indicating normal growth. In addition, liver, lung, and OM microsomal levels of several P450 proteins, including CYP1A, CYP2A, CYP2B, CYP2E, and CYP3A, were similar in *Cyp2f2*-null and WT mice, signifying absence of compensatory increases in the expression of these other *Cyp* genes in the *Cyp2f2*-null mice (Supplemental Fig. 1). Furthermore, the expression of CCSP, a developmental marker within the bronchiolar epithelium (Hackett and Gitlin, 1992), in various lung regions, including distal and mid-level airways and terminal bronchiolar, was found to be indistinguishable in *Cyp2f2*-null and WT mice (Supplemental Fig. 2), indicating absence of any obvious defects in lung development in the *Cyp2f2*-null mice.

Role of CYP2F2 in Microsomal NA Metabolic Activation In Vitro. The rates of NA-GSH formation in incubations with lung, liver, or OM microsomes were compared in *Cyp2f2*-null and WT mice, with NA used at a broad range of concentrations. Typical high performance liquid chromatogram, MS/MS spectrum, and calibration curve used for quantitation of NA-GSH are shown in Supplemental Data (Supplemental Fig. 3). Enzyme kinetic constants, estimated by nonlinear regression to Michaelis-Menten equation for either one- or two-component enzyme kinetics, as illustrated in a previous study (Siu and Tyndale, 2007), are shown in Table 1. The kinetic data are also shown as substrate-velocity curves (Supplemental Fig. 4). The involvement of more than one enzymatic component for lung and OM microsomes from WT mice was confirmed by the Eadie-Hofstee method (Fig. 2), through segmental linear regression; only a single component was detected for liver microsomes from WT mice or for lung, OM, and liver microsomes from the *Cyp2f2*-null mice. For the lung, the apparent K_m values were increased, whereas the apparent V_{max} values were decreased, in the *Cyp2f2*-null mice, compared with WT mice, resulting in a much (up to ~160-fold) lower catalytic efficiency toward NA. For liver and OM, the apparent catalytic efficiency values were also significantly decreased in the *Cyp2f2*-null mice, by ~3-fold and up to 16-fold, respectively; however, the V_{max} values were similar in the *Cyp2f2*-null and WT groups. These findings indicated that CYP2F2 is the major enzyme involved in NA bioactivation in the lung, at both high and low NA concentrations. In the liver and OM, CYP2F2 also contributed significantly to microsomal metabolism of NA, although the extent of CYP2F2's contribution was much less than in

TABLE 1

In vitro metabolism of NA in lung, liver, and OM microsomes from WT and *Cyp2f2*-null mice

Lung, liver, and OM microsomes were prepared from 2-month-old *Cyp2f2*-null and WT mice. Three batches of microsomes were used to determine the apparent enzyme kinetic constants (K_m and V_{max}), with each batch prepared from tissues pooled from five mice. The values reported are means ± S.D. (n = 3). The kinetic parameters were determined by nonlinear regression to Michaelis-Menten equation for either one- or two-component enzyme kinetics. Two enzymatic components were found for lung and OM microsomes from WT mice (thus yielding two sets of apparent K_m and V_{max} values); only a single component was detected for the other microsomal samples.

Strain & Tissue	K_m	V_{max}	V_{max}/K_m
	μM	$nmol \cdot min^{-1} \cdot mg\ protein^{-1}$	$ml \cdot mg\ protein^{-1} \cdot min^{-1}$
WT			
Lung	1.5 ± 0.2	0.5 ± 0.0	0.330
	34.3 ± 2.2	1.0 ± 0.3	0.029
Liver	17.4 ± 1.4	1.2 ± 0.1	0.069
OM	1.6 ± 0.3	0.5 ± 0.2	0.310
	74.5 ± 22.6	0.9 ± 0.2	0.012
Cyp2f2-null			
Lung	100 ± 20[a]	0.2 ± 0.0[a]	0.002
Liver	70.2 ± 12.4[b]	1.2 ± 0.3	0.017
OM	60.2 ± 11.0[c]	1.1 ± 0.0[d]	0.018

[a] $P < 0.01$ compared with either of the corresponding WT values.
[b] $P < 0.01$ compared with corresponding WT value.
[c] $P < 0.01$ compared with corresponding low-K_m WT value.
[d] $P < 0.01$ compared with corresponding low-K_m WT values.

the lung and became almost insignificant at high NA concentrations.

Role of CYP2F2 in NA Metabolism In Vivo. Pharmacokinetics of NA clearance was compared in *Cyp2f2*-null and WT mice with NA administered at 300 mg/kg i.p. Plasma NA reached maximal concentration at ~30 min after injection and then decreased quickly in both *Cyp2f2*-null and WT mice (Fig. 3A). In the *Cyp2f2*-null mice, NA clearance (as indicated by clearance/bioavailability value) was significantly decreased, accompanied by 2.8- and 3.4-fold increases in maximal concentration (C_{max}) and AUC values, respectively (Table 2). The formation of the GSH-trapped metabolite NA-GSH was also determined in both groups (Fig. 3B). Consistent with decreases in NA metabolism, the plasma levels of NA-GSH were substantially lower in the *Cyp2f2*-null than in WT mice, as indicated by 3.0- and 3.1-fold decreases in the C_{max} and AUC values, respectively (Table 2). These results show that CYP2F2 plays an important, although not absolute, role in NA clearance.

Given that CYP2F2 is expressed in both liver and the lung, we next assessed the relative contributions of lung and liver CYP2F2 to NA systemic metabolism by comparing NA metabolism in LCN mice (which have little microsomal P450 activity in the liver) and their WT littermates. We found that plasma NA levels were much higher in LCN than in WT mice treated with NA at 300 mg/kg (Fig. 3C; Table 2), a result indicating that hepatic P450 (presumably CYP2F2)-dependent NA metabolism is essential for the first-pass metabolism of intraperitoneally injected NA. It is noteworthy that the loss of hepatic P450 activity did not reduce the C_{max} or AUC for plasma levels of NA-GSH (Fig. 3D; Table 2), although the T_{max} seemed to be slightly increased. This latter result, which can be explained partly by the increased bio-

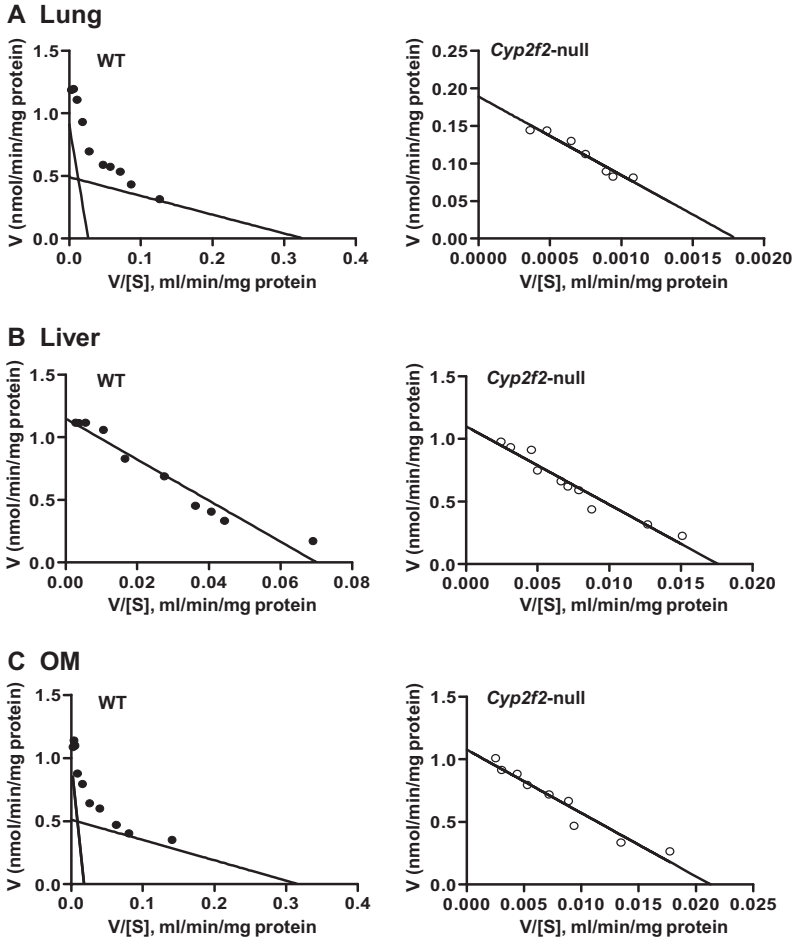

Fig. 2. Eadie-Hofstee plots for in vitro NA-GSH formation by lung (A), liver (B), and OM (C) microsomes. Contents of reaction mixtures are described under *Materials and Methods*. Microsomes were prepared from pooled OM, lungs, or livers from five 2-month-old male mice. The rates of NA-GSH formation were determined at various NA concentrations (2.5 to 400 μM). The data (means ± S.D., n = 3) were curve-fitted to the Michaelis-Menten equation. Substrate-velocity curves for the same kinetic data are shown in Supplemental Fig. 4. The calculated apparent kinetic parameters are shown in Table 1.

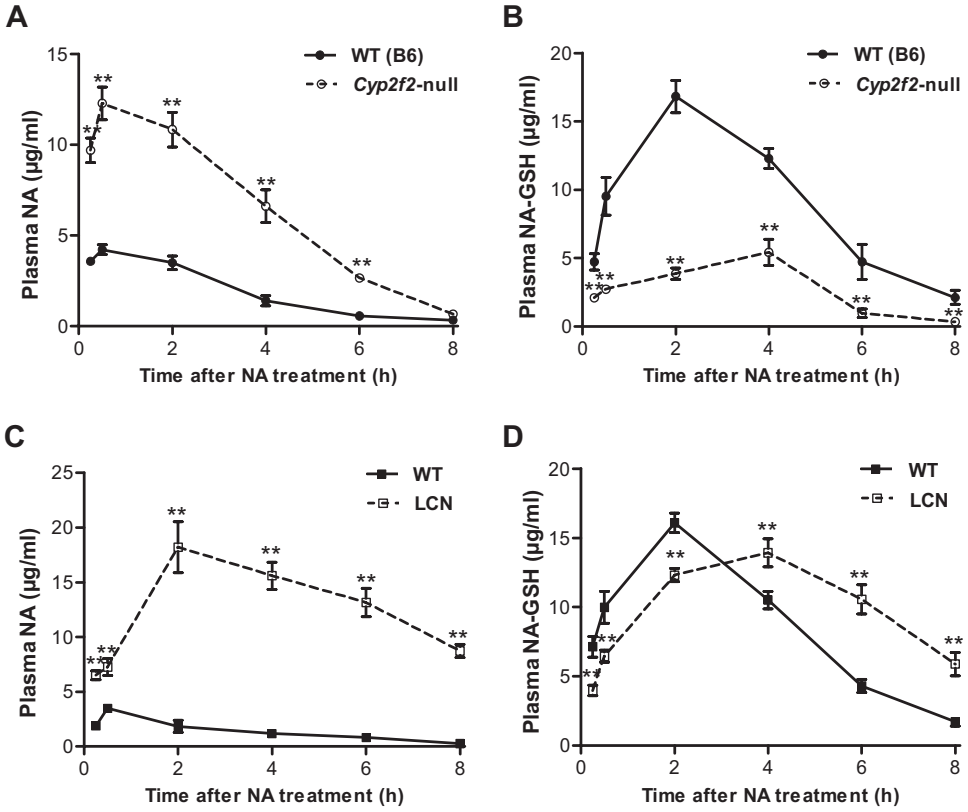

Fig. 3. Systemic levels of NA and NA-GSH at various times after NA treatment. Two-month-old, male, *Cyp2f2*-null mice (compared with WT B6 mice) and LCN mice (compared with their WT littermates) were treated with NA at 300 mg/kg i.p. Plasma was obtained at various times after dosing for determination of the levels of NA (A and C) and NA-GSH (B and D), as described under *Materials and Methods*. Data represent means ± S.D. (n = 4–6). **, $P < 0.01$ compared with levels in corresponding WT mice.

TABLE 2

Pharmacokinetic parameters for plasma NA and NA-GSH in mice treated with NA at 300 mg/kg

Values were derived from plots shown in Fig. 3. Data shown represent means ± S.D. [n = 6 for *Cyp2f2*-null and WT B6 (B6) control; n = 4 for LCN and WT littermate (WT) control].

Analyte & Strain	$AUC_{0-8\ h}$	$t_{1/2}$	CL/F	T_{max}	C_{max}
	$\mu g \cdot h^{-1} \cdot ml^{-1}$	h	ml/h	h	$\mu g/ml$
NA					
B6	15.0 ± 3.5	1.9 ± 0.4	394 ± 93	0.5 ± 0.1	4.3 ± 0.6
Cyp2f2-null	51.3 ± 10.1[a]	1.8 ± 0.3	116 ± 20[a]	0.5 ± 0.1	12.3 ± 2.2[a]
NA-GSH					
B6	75.1 ± 10.4	1.9 ± 0.6	N.A.	2.0 ± 0.0	16.8 ± 2.9
Cyp2f2-null	23.5 ± 5.2[a]	1.0 ± 0.3[a]	N.A.	4.0 ± 0.0[a]	5.7 ± 2.2[a]
NA					
WT	10.6 ± 2.1	2.3 ± 0.8	480 ± 95	0.5 ± 0.0	3.0 ± 1.4
LCN	110 ± 21[a]	5.1 ± 0.2[a]	36.1 ± 6.9[a]	2.0 ± 0.0[a]	18.2 ± 4.7[a]
NA-GSH					
WT	72.8 ± 5.0	1.5 ± 0.2	N.A.	2.0 ± 0.0	16.4 ± 1.4
LCN	81.5 ± 11.2	3.5 ± 1.0[a]	N.A.	3.0 ± 1.1	13.3 ± 2.5

N.A., not applicable; T_{max}, time at maximal concentration; $t_{1/2}$, elimination half-life.
[a] $P < 0.01$ compared with corresponding WT values.

availability of NA in the LCN mice, confirms that P450 enzymes in extrahepatic tissues (most probably the lung, where CYP2F2 is most abundant) are fully capable of producing reactive NA epoxides in vivo.

Role of CYP2F2 in the NA-Induced Tissue Toxicity. NA is known to induce respiratory tract toxicities, including observable lesions in the lung and OM, irrespective of the route of administration (Buckpitt et al., 2002). To determine the role of CYP2F2 in NA toxicity in vivo, we compared the extent of tissue toxicity in WT and *Cyp2f2*-null mice (Table 3; Fig. 4) treated with two known toxic NA doses (200 and 300 mg/kg i.p.; Plopper et al., 1992) at 24 h after dosing. NA-treated WT mice were less active than untreated or NA-treated *Cyp2f2*-null mice. In all NA-treated WT mice, tissue necrosis was clearly visible in the lung, at both NA doses, with evident detachment of both Clara cells and ciliated airway epithelial cells. In contrast, NA pneumotoxicity was apparently absent in most (five of six) of the NA-treated *Cyp2f2*-null mice dosed with NA at 300 mg/kg; even in the one *Cyp2f2*-null mouse exhibiting lesions, only minor toxicity was found. A further examination of high-resolution light micrographs revealed that, although the *Cyp2f2*-null mice treated at this dose had a few Clara cells with mild vacuolation of the cytoplasm, most of the remaining Clara cells had a normal appearance. Furthermore, none of the *Cyp2f2*-null mice treated with NA at 200 mg/kg exhibited obvious signs of pneumotoxicity (Table 3). Tissue toxicity was also detected in the olfactory regions of the nasal cavity of NA-treated mice; but there was no noticeable difference in the severity of toxicity in the *Cyp2f2*-null and WT mice. When dosed with

TABLE 3

NA toxicity in WT and *Cyp2f2*-null mice

Male 2-month-old WT and *Cyp2f2*-null mice were treated with a single injection of NA at either 200 or 300 mg/kg i.p. Histopathological analysis was conducted 24 h after the injection for lung, liver, and the olfactory region of nose. The severity of tissue damage was graded as follows: −, negative; ±, mild (for the lung, partial detachment of Clara cells from the bronchiolar epithelium; for the OM, slight detachment of mucosa and appearance of sloughed cells in the nasal cavity); +, moderate (for the lung, most Clara cells found to be necrotic and detached from the epithelium; for the OM, more extensive injury to the olfactory regions, evident as epithelial necrosis, detachment, sloughing, and ulceration).

NA Dose & Tissue	No. of Mice in Each Grade					
	WT			*Cyp2f2*-Null		
	−	±	+	−	±	+
200 mg/kg						
Liver	6	0	0	6	0	0
Lung	0	0	6	6	0	0
OM	2	3	1	0	5	1
300 mg/kg						
Liver	6	0	0	6	0	0
Lung	0	0	6	5	1	0
OM	0	0	6	0	1	5

NA at 300 mg/kg, both strains showed extensive injury to the OM, with evident epithelial necrosis, detachment, sloughing, and ulceration. When dosed with NA at 200 mg/kg, both strains exhibited minor cytotoxicity in the OM. No obvious hepatotoxicity was identified in either WT or *Cyp2f2*-null mice at either NA dose (data not shown).

Tissue NPSH levels, as an early marker of cytotoxicity (Phimister et al., 2004), were also determined for WT and *Cyp2f2*-null mice at 2 h after NA dosing at 300 mg/kg (Table 4). Corn oil was used as vehicle control. Consistent with the results of pathological examination at 24 h after NA treatment, there was no significant decrease in lung NPSH levels in NA-treated compared with vehicle-treated *Cyp2f2*-null mice at 2 h after NA dosing, whereas a 40% decrease in lung NPSH levels was found in NA-treated WT mice. For the OM, NPSH levels decreased by ~85% in both mouse strains after NA treatment compared with vehicle controls, confirming the earlier conclusion from the histopathological data that CYP2F2 does not play a significant role in NA-induced nasal toxicity at the doses studied. For the liver, NPSH levels decreased by ~83% in WT mice and ~70% in *Cyp2f2*-null mice after NA treatment compared with corresponding vehicle-treated mice, consistent with a relatively minor role of CYP2F2 in hepatic NA metabolic activation.

Tissue levels of NA and NA-GSH were also determined in lung, liver, and OM, at 2 h after NA treatment (Table 5). Consistent with the NPSH data, the loss of CYP2F2 was associated with a 77% decrease in NA-GSH levels and 70% increase in NA level (compared with WT mice) in the lung; however, it had only marginal effects on liver NA-GSH or NA levels and had essentially no effects on NA-GSH or NA levels in the OM. Taken together, these results indicate that lung CYP2F2 plays the most important role in NA metabolic activation in the lung and in NA-induced pneumotoxicity, whereas the role of CYP2F2 in NA metabolic activation and cytotoxicity in the OM is negligible.

Discussion

A novel knockout mouse model targeting the *Cyp2f2* gene is described here for the first time. The *Cyp2f2*-null mouse joins three other mouse models reported to target members of the *Cyp2* gene clusters on mouse chromosome 7: the *Cyp2g1*-null/*Cyp2a5*-low model (Zhuo et al., 2004), the *Cyp2a5*-null model (Zhou et al., 2010), and the *Cyp2g1*-null mouse model (Zhou et al., 2011). As with *Cyp2a5*-null and *Cyp2g1*-null models, the *Cyp2f2*-null mouse was generated on a B6 genetic background. Homozygous *Cyp2f2*-null mice were fertile and had no discernible differences from WT mice in body weight, growth rate, and major organ weight; these phenotypes were not unexpected given the fact that there has been no endogenous substrate identified for any of the CYP2F

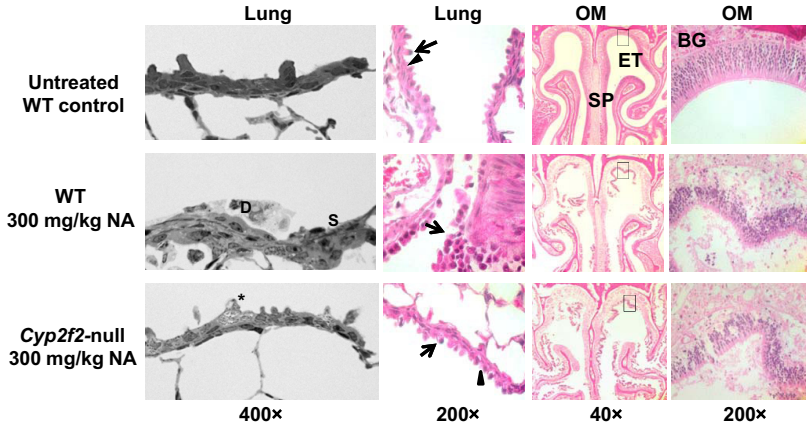

Fig. 4. NA-induced toxicity in WT and *Cyp2f2*-null mice. Two-month-old male mice were either untreated or treated with a single injection of NA in corn oil at 300 mg/kg i.p. for WT and *Cyp2f2*-null (Null) mice. Tissues (lung and nose) were obtained for histopathological examination at 24 h after NA treatment. For the lung, representative hematoxylin and eosin-stained sections (200×) and high-resolution light micrographs (400×) are shown. Untreated WT and Null (not shown) mice had a normal bronchiolar epithelium; NA-treated WT mice showed necrosis and detachment of Clara cells (arrow) and ciliated cells (arrow head) from the epithelium, with abundant cell debris (D) present in the airway lumen and the remaining cells squamated (S) shown in the high-resolution micrograph; treated Null mice exhibited almost normal epithelium as seen in untreated WT or Null mice, with a few Clara cells mildly vacuolated (*) shown in the high resolution micrograph. For the nose, hematoxylin and eosin-stained cross-sections of the nasal cavity obtained at the level 3 of Young (1981) are shown; boxed areas, at the dorsal medial meatus, in the middle panel (40×) are shown at 200× on the right. Untreated WT and Null mice had normal ethmoidal turbinates (ET) lined by a thick, pseudostratified olfactory neuroepithelium, with Bowman's glands (BG) in the submucosa. NA-treated WT mice displayed signs of acute olfactory epithelial injury, including detachment of the mucosa and the appearance of sloughed cells in the nasal cavity; treated Null mice also had extensive injury to the olfactory regions, evident as epithelial necrosis, detachment, sloughing, and ulceration. SP, nasal septum.

TABLE 4

NPSH levels in lung, liver, and OM of vehicle- or NA-treated mice

Two-month-old male WT and Cyp2f2-null (Null) mice were given a single injection of NA at 300 mg/kg i.p. Tissues were collected from individual mice at 2 h after dosing. The data represent means ± S.D. (n = 3). NA-induced NPSH decrease was calculated as (V − N)/V × 100%.

Tissues & Strain	NPSH Level		NA-Induced NPSH Decrease
	Vehicle-Treated	NA-Treated	
	μmol/g tissue		*%*
Lung			
WT	1.14 ± 0.19	0.68 ± 0.04[a]	40
Null	1.02 ± 0.14	0.95 ± 0.05[b]	7
Liver			
WT	7.40 ± 0.71	1.23 ± 0.12[a]	83
Null	7.12 ± 0.58	2.15 ± 0.17[a,b]	70
OM			
WT	1.97 ± 0.12	0.29 ± 0.03[a]	85
Null	2.19 ± 0.21	0.29 ± 0.03[a]	87

V, vehicle-treated; N, NA-treated.
[a] $P < 0.01$ NA treatment compared with corresponding vehicle control values.
[b] $P < 0.01$ Null compared with corresponding WT values.

TABLE 5

NA and NA-GSH levels in lung, liver, and OM of NA-treated mice

Two-month-old male WT and *Cyp2f2*-null (Null) mice were given a single injection of NA at 300 mg/kg i.p. Tissues were collected from individual mice 2 h after dosing. The data represent means ± S.D. (n = 3).

Tissues & Strain	NA Level	Null/WT	NA-GSH Level	Null/WT
	μg/g tissue	*%*	*μg/g tissue*	*%*
Lung				
WT	12.1 ± 2.5		106 ± 13	
Null	20.9 ± 3.9[a]	173	24.5 ± 4.5[a]	23
Liver				
WT	17.6 ± 2.9		142 ± 16	
Null	23.6 ± 2.6	134	118 ± 3	83
OM				
WT	0.7 ± 0.1		4.3 ± 1.2	
Null	0.6 ± 0.3	86	5.6 ± 1.7	130

[a] $P < 0.01$ Null compared with corresponding WT values.

enzymes, and they also affirm that the insertion of neo in place of the *Cyp2f2* fourth exon did not cause any adverse effect on development, reproduction, or growth. The presence of neo (and the loss of CYP2F2) did not seem to affect the expression of neighboring *Cyp2a* or *Cyp2b* genes or that of several other P450 genes examined, in contrast to the neighboring effect seen previously in the *Cyp2g1*-null/*Cyp2a5*-low model (Zhuo et al., 2004). In that regard, *Cyp2f2* is flanked by two P450 pseudogenes: *Cyp2a20-ps* on the 5′ side and *Cyp2t4* on the 3′ side (Wang et al., 2003), which might have served to insulate any effects of the neo transcription on more peripheral genes.

Our finding that NA-induced lung injury is essentially abolished in the *Cyp2f2*-null mouse confirms the long-held suspicion that CYP2F2 plays a critical role in the high sensitivity of mouse lung to NA toxicity (Buckpitt et al., 2002; Cruzan et al., 2009). Our finding that NA toxicity in the OM was essentially unaffected by the loss of CYP2F2 is also interesting, as it illustrates the complexity of the metabolic mechanisms underlying site selective respiratory tract toxicity of xenobiotic compounds. The tissue difference in the impact of CYP2F2 loss on NA-induced toxicity is consistent with in vitro metabolic data, which showed a huge (~160-fold) decrease in lung but only a modest (~16-fold) decrease in OM, in the apparent catalytic efficiencies toward NA bioactivation. Thus, although CYP2F2 is abundant in both lung and OM, other P450 enzymes seem to play a more active role in NA bioactivation in the OM, at least under the dose and substrate concentrations tested. In that regard, CYP2F2 might play a more active role in NA bioactivation in the OM at very low substrate concentrations, given the enzyme kinetic data indicating the apparent loss of a low-K_m component in OM (as well as lung) of the *Cyp2f2*-null mice. Studies are under way to determine the contributions of other P450 enzymes, particularly CYP2A5 [which is highly abundant in the mouse OM (Gu et al., 1998)], to NA bioactivation and toxicity in the OM.

It is well recognized that NA induces respiratory tract cytotoxicity in rodents irrespective of the route of administration (Plopper et al., 1992; West et al., 2001). In the present study, the intraperitoneal route was used according to assay conditions previously established for testing acute respiratory tract toxicity in mice (Plopper et al., 1992). It is conceivable that the *Cyp2f2*-null mouse will be likewise resistant to NA-induced lung toxicity in other exposure models, because the routes of exposure will change only the internal dose available for bioactivation, not the presence of the highly abundant CYP2F2 in the lungs for target tissue NA metabolic activation.

CYP2F2 is expressed in the mouse liver as well as in the respiratory tract, the concentration of CYP2F2 protein being comparable in liver and lung microsomes. Our finding that clearance of intraperitoneally injected NA was significantly decreased in both the *Cyp2f2*-null mouse and the LCN mouse indicates that hepatic CYP2F2 plays an essential role in the first-pass metabolism of parenteral NA. It is likely that lung CYP2F2 would play a more critical role in the metabolic disposition of inhaled NA than in the clearance of parenteral administered NA, given the location of the lung at the portal of entry; the extent of CYP2F2's contribution in that regard remains to be determined experimentally. It is noteworthy that NA absorption and systemic distribution are expected to be rapid, and thus hepatic contribution to systemic clearance of inhaled NA is also likely.

It is noteworthy that whereas the decrease in NA clearance in the *Cyp2f2*-null mouse was accompanied by a comparable decrease in the levels of NA-GSH, a marker for reactive NA metabolites produced in vivo, the decreased NA clearance in the LCN mouse was not accompanied by a corresponding decrease in plasma NA-GSH. These data support the idea that lung CYP2F2 is sufficient for mediating NA metabolic activation and lung toxicity and that it also contributes to systemic formation of NA-GSH. However, it remains to be determined whether liver-generated reactive NA metabolites contribute to NA-induced lung or nasal toxicity in WT mice.

The *Cyp2f2*-null mouse model will probably have broad applications for studying the toxicity of other chemicals that are CYP2F substrates. In addition to NA, CYP2F enzymes also metabolize numerous other lung toxicants, such as 3-methylindole, styrene, and trichloroethylene (see Zhang and Ding, 2008), for which human risks of lung toxicity remain unclear. In that regard, preliminary studies on styrene toxicity in the *Cyp2f2*-null mice have been reported indicating that CYP2F2 also plays a critical role in the lung toxicity of styrene in mice (Cruzan et al., 2011).

The demonstration of a critical role of CYP2F2 in NA-induced lung toxicity in mice prompts the question of whether the human ortholog, CYP2F1, is also important for

NA metabolic activation in humans. However, although both human lung and human liver can metabolize NA (Buckpitt and Bahnson 1986; Cho et al., 2006), the role of human CYP2F1 in NA bioactivation is not well understood, in large part because of repeated failures in multiple laboratories to produce functional CYP2F1 through heterologous expression and a lack of knowledge about the distribution and function of CYP2F1 in the human lung. Indeed, the potential for NA to cause cytotoxic effects in the human lung remains undefined. The availability of the *Cyp2f2*-null mouse will make it possible to generate a CYP2F1-humanized mouse model to directly determine the capability of human CYP2F1 to bioactivate NA and other potential lung toxicants in vivo. Efforts to develop such a mouse model are under way.

Although our data are conclusive in demonstrating the important role of CYP2F2 in NA-induced lung toxicity, it remains to be determined whether, under certain conditions, NA metabolism by mouse P450s other than CYP2F2 can mediate NA toxicity in *Cyp2f2*-null lungs, which may serve as a model for human lungs with little CYP2F1 expression or activity, but express other P450 enzymes, such as CYP1A1 (van Bladeren et al., 1985) and CYP2A13 (Fukami et al., 2008), that are capable of bioactivating NA. The conditions that may enhance the participation of the less efficient P450 enzymes in NA bioactivation in vivo include higher NA doses, which may occur when NA exposure is through inhalation or dermal absorption (thus bypassing first-pass metabolism by the digestive organs) and a higher expression level of the P450 enzymes as a result of site-specific enrichment in select lung regions, as demonstrated previously (Buckpitt et al., 1995). In addition, NA toxicity was examined only at 24 h after dosing in the present study. Lung toxicity might be detected in the *Cyp2f2*-null mice at a later time.

In summary, a novel *Cyp2f2*-null mouse model was generated and characterized in this study. The mouse model has been found to be ideal for determination of the roles of CYP2F2 in xenobiotic metabolism and toxicity in vivo. Initial application of the *Cyp2f2*-null mouse model to studies on NA, an important environmental chemical and respiratory tract toxicant, led to the novel and definitive finding that mouse CYP2F2 plays an essential role in the bioactivation and toxicity of NA in the lung but not in the OM. The *Cyp2f2*-null mouse should be valuable for studies on the role of CYP2F2 in the metabolism and toxicity of numerous other xenobiotic compounds, and for future production of a *CYP2F1*-humanized mouse.

Acknowledgments

We thank Drs. Alan Buckpitt and Dexter Morin of UC Davis for providing NA-GSH standards, Dr. Rachel Tyndale of the University of Toronto for helpful discussion, and Weizhu Yang for technical assistance. We gratefully acknowledge the use of the Transgenic and Knockout Mouse Core, the Histopathology Core, and the Advanced Light Microscopy and Image Analysis Core Facilities of the Wadsworth Center and the University of Michigan Transgenic Animal Model Core.

Authorship Contributions

Participated in research design: Li, Wei, Van Winkle, Zhang, and Ding.

Conducted experiments: Li, Wei, Van Winkle, Zhou, Hu, Xie, and Kluetzman.

Contributed new reagents or analytic tools: Zhang.

Performed data analysis: Li, Van Winkle, and Ding.

Wrote or contributed to the writing of the manuscript: Li, Wei, Van Winkle, Zhang, and Ding.

References

Abdo K, Eustis S, McDonald M, Jokinen M, Adkins B, and Haseman J (1992) Naphthalene: a respiratory tract toxicant and carcinogen for mice. *Inhal Toxicol* **4:**393–409.

Abdo KM, Grumbein S, Chou BJ, and Herbert R (2001) Toxicity and carcinogenicity study in F344 rats following 2 years of whole-body exposure to naphthalene vapors. *Inhal Toxicol* **13:**931–950.

Arey J, Sielinska B, Atkinson R, and Winer A (1987) Polycyclic aromatic hydrocarbon and nitroarene concentrations in ambient air during a wintertime high NOx episode in the Los Angeles basin. *Atmos Environ* **21:**1437–1444.

Bartha B, Huber C, Harpaintner R, and Schroder P (2010) Effects of acetaminophen in *Brassica juncea* L. Czern.: investigation of uptake, translocation, detoxification, and the induced defense pathways. *Environ Sci Pollut Res Int* **17:**1553–1562.

Brusick D (2008) Critical assessment of the genetic toxicity of naphthalene. *Regul Toxicol Pharmacol* **51:**S37–S42.

Buckpitt A, Boland B, Isbell M, Morin D, Shultz M, Baldwin R, Chan K, Karlsson A, Lin C, Taff A, et al. (2002) Naphthalene-induced respiratory tract toxicity: metabolic mechanisms of toxicity. *Drug Metab Rev* **34:**791–820.

Buckpitt A, Chang AM, Weir A, Van Winkle L, Duan X, Philpot R, and Plopper C (1995) Relationship of cytochrome P450 activity to Clara cell cytotoxicity. IV. Metabolism of naphthalene and naphthalene oxide in microdissected airways from mice, rats, and hamsters. *Mol Pharmacol* **47:**74–81.

Buckpitt AR and Bahnson LS (1986) Naphthalene metabolism by human lung microsomal enzymes. *Toxicology* **41:**333–341.

Buckpitt AR, Castagnoli N Jr, Nelson SD, Jones AD, and Bahnson LS (1987) Stereoselectivity of naphthalene epoxidation by mouse, rat, and hamster pulmonary, hepatic, and renal microsomal enzymes. *Drug Metab Dispos* **15:**491–498.

Buckpitt AR and Warren DL (1983) Evidence for hepatic formation, export and covalent binding of reactive naphthalene metabolites in extrahepatic tissues in vivo. *J Pharmacol Exp Ther* **225:**8–16.

Cho TM, Rose RL, and Hodgson E (2006) In vitro metabolism of naphthalene by human liver microsomal cytochrome P450 enzymes. *Drug Metab Dispos* **34:**176–183.

Cruzan G, Bus J, Banton M, Gingell R, and Carlson G (2009) Mouse specific lung tumors from CYP2F2-mediated cytotoxic metabolism: an endpoint/toxic response where data from multiple chemicals converge to support a mode of action. *Regul Toxicol Pharmacol* **55:**205–218.

Cruzan G, Bus J, Ding X, Hotchkiss J, Harkema J, and Gingell R (2011) No lung toxicity from styrene in CYP2F2 knockout mice (Abstract). *Toxicol Sci* **120** (**Suppl 2):**566.

Ding XX and Coon MJ (1990) Immunochemical characterization of multiple forms of cytochrome P-450 in rabbit nasal microsomes and evidence for tissue-specific expression of P-450s NMa and NMb. *Mol Pharmacol* **37:**489–496.

Fukami T, Katoh M, Yamazaki H, Yokoi T, and Nakajima M (2008) Human cytochrome P450 2A13 efficiently metabolizes chemicals in air pollutants: naphthalene, styrene, and toluene. *Chem Res Toxicol* **21:**720–725.

Gu J, Cui H, Behr M, Zhang L, Zhang QY, Yang W, Hinson JA, and Ding X (2005) In vivo mechanisms of tissue-selective drug toxicity: effects of liver-specific knockout of the NADPH-cytochrome P450 reductase gene on acetaminophen toxicity in kidney, lung, and olfactory mucosa. *Mol Pharmacol* **67:**623–630.

Gu J, Walker VE, Lipinskas TW, Walker DM, and Ding X (1997) Intraperitoneal administration of coumarin causes tissue-selective depletion of cytochrome P450 and cytotoxicity in the olfactory mucosa. *Toxicol Appl Pharmacol* **146:**134–143.

Gu J, Weng Y, Zhang QY, Cui H, Behr M, Wu L, Yang W, Zhang L, and Ding X (2003) Liver-specific deletion of the NADPH-cytochrome P450 reductase gene: impact on plasma cholesterol homeostasis and the function and regulation of microsomal cytochrome P450 and heme oxygenase. *J Biol Chem* **278:**25895–25901.

Gu J, Zhang QY, Genter MB, Lipinskas TW, Negishi M, Nebert DW, and Ding X (1998) Purification and characterization of heterologously expressed mouse CYP2A5 and CYP2G1: role in metabolic activation of acetaminophen and 2,6-dichlorobenzonitrile in mouse olfactory mucosal microsomes. *J Pharmacol Exp Ther* **285:**1287–1295.

Hackett BP and Gitlin JD (1992) Cell-specific expression of a Clara cell secretory protein-human growth hormone gene in the bronchiolar epithelium of transgenic mice. *Proc Natl Acad Sci* **89:**9079–9083.

Hukkanen J, Pelkonen O, Hakkola J, and Raunio H (2002) Expression and regulation of xenobiotic-metabolizing cytochrome P450 (CYP) enzymes in human lung. *Crit Rev Toxicol* **32:**391–411.

Köntgen F, Süss G, Stewart C, Steinmetz M, and Bluethmann H (1993) Targeted disruption of the MHC class II Aa gene in C57BL/6 mice. *Int Immunol* **5:**957–964.

Lin CY, Wheelock AM, Morin D, Baldwin RM, Lee MG, Taff A, Plopper C, Buckpitt A, and Rohde A (2009) Toxicity and metabolism of methylnaphthalenes: comparison with naphthalene and 1-nitronaphthalene. *Toxicology* **260:**16–27.

Phimister AJ, Lee MG, Morin D, Buckpitt AR, and Plopper CG (2004) Glutathione depletion is a major determinant of inhaled naphthalene respiratory toxicity and naphthalene metabolism in mice. *Toxicol Sci* **82:**268–278.

Plopper CG, Suverkropp C, Morin D, Nishio S, and Buckpitt A (1992) Relationship of cytochrome P-450 activity to Clara cell cytotoxicity. I. Histopathologic comparison of the respiratory tract of mice, rats and hamsters after parenteral administration of naphthalene. *J Pharmacol Exp Ther* **261:**353–363.

Shultz MA, Choudary PV, and Buckpitt AR (1999) Role of murine cytochrome P-450 2F2 in metabolic activation of naphthalene and metabolism of other xenobiotics. *J Pharmacol Exp Ther* **290:**281–288.

Siu EC and Tyndale RF (2007) Characterization and comparison of nicotine and

cotinine metabolism in vitro and in vivo in DBA/2 and C57BL/6 mice. *Mol Pharmacol* **71:**826–834.
Tonge RP, Kelly EJ, Bruschi SA, Kalhorn T, Eaton DL, Nebert DW, and Nelson SD (1998) Role of CYP1A2 in the hepatotoxicity of acetaminophen: investigations using Cyp1a2 null mice. *Toxicol Appl Pharmacol* **153:**102–108.
van Bladeren PJ, Sayer JM, Ryan DE, Thomas PE, Levin W, and Jerina DM (1985) Differential stereoselectivity of cytochromes P-450b and P-450c in the formation of naphthalene and anthracene 1,2-oxides. The role of epoxide hydrolase in determining the enantiomer composition of the 1,2-dihydrodiols formed. *J Biol Chem* **260:**10226–10235.
Wang H, Donley KM, Keeney DS, and Hoffman SM (2003) Organization and evolution of the *Cyp2* gene cluster on mouse chromosome 7, and comparison with the syntenic human cluster. *Environ Health Perspect* **111:**1835–1842.
Warren DL, Brown DL Jr., and Buckpitt AR (1982) Evidence for cytochrome P-450 mediated metabolism in the bronchiolar damage by naphthalene. *Chem Biol Interact* **40:**287–303.
Weng Y, Fang C, Turesky RJ, Behr M, Kaminsky LS, and Ding X (2007) Determination of the role of target tissue metabolism in lung carcinogenesis using conditional cytochrome P450 reductase-null mice. *Cancer Res* **67:**7825–7832.
West JA, Pakehham G, Morin D, Fleschner CA, Buckpitt AR, and Plopper CG (2001) Inhaled naphthalene causes dose dependent Clara cell cytotoxicity in mice but not in rats. *Toxicol Appl Pharmacol* **173:**114–119.
Xie F, Zhou X, Behr M, Fang C, Horii Y, Gu J, Kannan K, and Ding X (2010) Mechanisms of olfactory toxicity of the herbicide 2,6-dichlorobenzonitrile: essential roles of CYP2A5 and target-tissue metabolic activation. *Toxicol Appl Pharmacol* **249:**101–106.
Young JT (1981) Histopathologic examination of the rat nasal cavity. *Fundam Appl Toxicol* **1:**309–312.
Zhou X, Wei Y, Xie F, Laukaitis CM, Karn RC, Kluetzman K, Gu J, Zhang QY, Roberts DW, and Ding X (2011) A novel defensive mechanism against acetaminophen toxicity in the mouse lateral nasal gland: role of CYP2A5-mediated regulation of testosterone homeostasis and salivary androgen-binding protein expression. *Mol. Pharmacol* **79:**710–723.
Zhou X, Zhuo X, Xie F, Kluetzman K, Shu YZ, Humphreys WG, and Ding X (2010) Role of CYP2A5 in the clearance of nicotine and cotinine: insights from studies on a Cyp2a5-null mouse model. *J Pharmacol Exp Ther* **332:**578–587.
Zhuo X, Gu J, Behr MJ, Swiatek PJ, Cui H, Zhang QY, Xie Y, Collins DN, and Ding X (2004) Targeted disruption of the olfactory mucosa-specific *Cyp2g1* gene: impact on acetaminophen toxicity in the lateral nasal gland, and tissue-selective effects on *Cyp2a5* expression. *J Pharmacol Exp Ther* **308:**719–728.
Zhang QY and Ding X (2008) The CYP2F, CYP2G and CYP2J subfamilies, in *Cytochrome P450: Role in the Metabolism and Toxicity of Drugs and Other Xenobiotics* (Ioannides C ed), pp 309–353, RSC Publishing, Cambridge, UK.

Address correspondence to: Dr. Xinxin Ding, Wadsworth Center, New York State Department of Health, Empire State Plaza, Box 509, Albany, NY 12201-0509. E-mail: xding@wadsworth.org